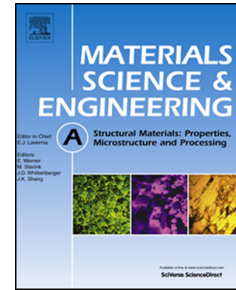


Journal Pre-proof

Collapse of helium-filled voids in extreme deformation: Dislocation mechanisms

R.M. Flanagan, M.A. Meyers, S.M. Valone, S.J. Fensin



PII: S0921-5093(22)00120-4

DOI: <https://doi.org/10.1016/j.msea.2022.142712>

Reference: MSA 142712

To appear in: *Materials Science & Engineering A*

Received Date: 29 April 2021

Revised Date: 16 December 2021

Accepted Date: 19 January 2022

Please cite this article as: R.M. Flanagan, M.A. Meyers, S.M. Valone, S.J. Fensin, Collapse of helium-filled voids in extreme deformation: Dislocation mechanisms, *Materials Science & Engineering A* (2022), doi: <https://doi.org/10.1016/j.msea.2022.142712>.

This is a PDF file of an article that has undergone enhancements after acceptance, such as the addition of a cover page and metadata, and formatting for readability, but it is not yet the definitive version of record. This version will undergo additional copyediting, typesetting and review before it is published in its final form, but we are providing this version to give early visibility of the article. Please note that, during the production process, errors may be discovered which could affect the content, and all legal disclaimers that apply to the journal pertain.

© 2022 Published by Elsevier B.V.

RMF, MAM, SMV, SJF: Conceptualization, Methodology, Investigation, Reviewing, Editing
RMF, SJF: Software, Visualization, Validation **RMF:** Original draft preparation **MAM, SJF:**
Supervision

Journal Pre-proof

Collapse of Helium-filled Voids in Extreme Deformation: Dislocation Mechanisms

R.M. Flanagan¹, M.A. Meyers¹, S.M. Valone², and S.J. Fensin^{2,*}

1. University of California, San Diego, CA

2. Los Alamos National Laboratory, Los Alamos, NM

* Corresponding Author

Abstract

The mechanisms responsible for the collapse of helium-filled bubbles during the passage of shock waves in monocrystalline copper are revealed. Both internal pressure (caused by pre-existing helium atoms) and bubble size are varied in molecular dynamics simulations to understand the atomistic scale deformation as they are subjected to shock compression at pressures of 48, 123, and 170 GPa, corresponding to particle velocities of 1.0, 2.0, and 2.5 km/s. Both empty and helium filled bubbles serve as dislocation sources, generating intense, localized plastic regions. There are distinct differences in the collapse of empty voids compared to He-filled bubbles, the former requiring less stress and generating a greater density of dislocations for a given shock strength. A generalized model for dislocation emission is proposed, where the inclusion of shear stress generated by the helium bubble increases the critical stress to generate dislocations at the defect surface, demonstrating the change in plastic deformation.

Key words: copper alloys, plasticity, modelling/simulations

Correspondence should be addressed to Saryu Fensin at saryuj@lanl.gov

1. Introduction

When a material is subjected to shock compression, a state of uniaxial strain is induced, generating shear stresses that are a significant fraction of the applied stress. These, in-turn, activate the mechanisms by which materials deform in this extreme regime. The behavior of a material under shock loading is greatly influenced by its structure and composition, with factors such as grain size, texture, porosity, and other defects altering the mechanisms of deformation. All real materials contain a significant number of defects, such as vacancies, impurities, dislocations, grain boundaries, and voids. These defects may act as initiation sites for damage, due to the intense plastic deformation around them and by acting as sites for cracking.

The study of the role of pre-existing defects during shock loading presents special challenges due to the required spatiotemporal resolution to probe such rapid and small-scale phenomena. Microstructure, including pre-existing defects clearly affects the dynamic behavior of materials [1]–[6]. For example, vacancies, impurities, dislocations, and shock-induced phase changes may activate heterogeneous dislocation nucleation, decrease the shock stress needed to initiate plasticity, induce shock melting, influence twinning behavior, and alter the dynamic strength of a material [7]–[16]. Grain boundaries have been studied extensively as sources and sinks of dislocations due to the interplay between grain size, strain rate, and material strength [17]–[35]; defects interact heavily with grain boundaries. Larger pre-existing heterogeneities such as second-phase particles and inclusions have also been linked to changes in damage nucleation mechanisms and spall strength [36]–[43], [44].

Considerable research has been done to understand the behavior of voids under shock loading, especially due to substantial interest in porous and explosive media, where voids can generate hot spots and initiate detonation [45]–[50]. In spalling generated by the reflection of shock

waves at free surfaces, the nucleation, growth, and coalescence of voids has been well-studied, with significant evidence pointing to void growth via dislocation emission as the mechanism of deformation [34], [51]–[59]. For collapsing voids, a description of their constitutive behavior under shock compression has helped elucidate the shock behavior of distended materials [60], [61]. Simulations show that dislocation loops emitted during void collapse are shear loops, with intense local plasticity being generated for voids in proximity to one another [62]–[64]. The development of shear loops has been linked to geometrically necessary dislocations, demonstrating that as a cavity collapses, shear dislocation loops carry vacancies away from the void, thus coupling the processes of compaction and plasticity [65]. Wilkerson and Ramesh [66] incorporated dislocation dynamics and, in particular, drag, relativistic effects, and their evolving density and were able to explain the anomalous temperature sensitivity of spall strength. They obtained a closed form solution by incorporating dislocation emission from a nanosized void surface under extreme loading rates [67]. This approach generalizes the Lubarda et al. [68], [69] treatment and has a powerful predictive capability that extends to different strain rates, stress states, temperature, void size and porosity.

Whereas the size effect in the Tang et al. [70] analysis comes from the radius of the dislocation loop at the emission as well as image forces, the approach by Wilkerson and Ramesh [67] uses the surface energy. These equations were later generalized to incorporate a distribution of void sizes and compared with molecular dynamics (MD) calculations [71]. Nitol et al. [71] conducted MD calculations that predict the spall strength of magnesium and magnesium-aluminum alloys which show the dislocation emission from voids with a diameter of 4 nm. The dislocation configurations resemble the ones obtained in the current research. In addition to these

developments, Lubarda investigated analytically the effect of combined loading [68] and the image forces [69].

Specific interest in voids filled with He (He bubbles) has grown due to the extreme environments where helium damage may be induced, such as fusion reactors and spacecrafts. Such environments degrade material properties via irradiation, generating vacancies, voids, and dislocations [72]–[74], as well as helium defects due to its low solubility in metals such as copper [75], [76]. Helium has been shown to cause embrittlement, swelling and hardening [72], [76]–[80] and may play an important role in material strength. As such, helium-implanted materials under shock loading [81]–[86] have become particularly interesting. Atomistic scale studies are especially useful for studying helium defects because they effectively model the helium bubbles at physically relevant length scales and also provide an extreme case for impedance mis-match between defects and bulk material. This study aims to better understand the atomistic scale processes of deformation when copper, seeded with He-filled voids, is subjected to shock compression.

2. Methodology

Molecular dynamics (MD) simulations provide the appropriate spatial and temporal resolution to study the nanoscale behavior of voids, both empty and He-filled, under shock compression. The role of void size and internal pressure in dictating the dynamic response of a $\langle 111 \rangle$ single crystal copper was investigated in this work using the Large-scale Atomic/Molecular Massively Parallel Simulator (LAMMPS) [87]. Cu was selected as a model FCC material due to its extensively characterized interatomic potentials and lack of phase transitions to complicate the observed behaviors. All interatomic interactions for Cu-Cu and Cu-He were described using a splined EAM potential developed by Demkowicz et. al [88]. The Equation of State (EOS) for

Helium in this potential matches that measured experimentally in reference [89]. Quantitative analysis of generated defects under shock compression and visualization was performed using OVITO [90]. Single crystal copper was oriented such that the x, y, and z axes correspond to the $[1\bar{1}0]$, $[111]$, and $[11\bar{2}]$ crystallographic directions with dimensions of 50.0 nm by 125.0 nm by 50.0 nm for a total of 26.9 million atoms. The simulation cell is periodic in the x and z directions.

The goal of this study was to determine the interplay between initial bubble size and initial bubble pressure as it impacts the dynamic behavior of materials. To achieve this goal, it was important to perform systematic simulations where only one parameter at a time was changed. Hence, in this work only a single bubble was added to the simulation cell by selecting and deleting a spherical region of copper with a specified radius centered at a depth of 20 nm from the free surface. The radius of the bubble was varied from 2 to 9 nm while the internal pressure was held constant. Since the goal of the study was to also investigate the role of internal pressure on the collapse of these voids, the pressure was varied from 0 to 2.39 GPa for a given bubble size. To create a zero internal pressure within the bubble, the spherical defect was initially left empty; we will refer to this zero-pressure bubble as a void from now-onwards. Addition of helium atoms increased the internal pressure; this was done by embedding an FCC lattice of helium with a lattice constant of 0.424 nm (inducing an internal pressure of 1.35 GPa) or a lattice constant of 0.354 nm (inducing an internal pressure of 2.39 GPa) into the single bubble. It is important to note that the size of the helium bubbles can vary from 1-2 nm to up to 8-10 nm. However, not much information is available regarding helium bubble pressure. Hence, this study attempts to determine how internal pressure changes for the helium bubble would affect its ability to nucleate dislocations under shock. The point is to investigate if there an effect and not the actual internal pressure values used in this work. Any copper atoms that overlapped with the helium atoms were deleted.

Throughout this paper, we refer to samples containing helium bubbles with an initial internal pressure of 1.35 GPa as Cu-He-1.35 while samples containing helium bubbles with an initial internal pressure of 2.39 GPa as Cu-He-2.39. The initial internal pressure of the bubble contained in each sample was calculated by dividing the trace of the stress tensor, where each diagonal component is the sum of kinetic energy and intra/intermolecular interactions, by the sum of per-atom Voronoi volumes. The simulation cell used in this study is shown in Figure 1.

After the addition of the bubble, the system was equilibrated using a Nosé-Hoover isobaric-isothermal ensemble (NPT) at a pressure of 0 MPa at 300 K for 10 ps. Following equilibration, the system was shocked along the y axis using a momentum mirror [91] at particle velocities of 1.0, 2.0, and 2.5 km/s, which correspond to peak shock stresses of 48, 123, and 170 GPa, respectively. Measurements such as material temperature, stress, and potential energy were obtained via LAMMPS simulations and visualized in OVITO [90]. Dislocations were identified and quantified using the Dislocation Extraction Algorithm (DXA) [92] as the shock front moved through the material. To ensure accurate comparison to future experimental work (to be performed via gas gun experiments at LANL), where helium bubbles are too small to be detected by any of the currently available diagnostics, the analysis focused on the behavior of copper atoms.

3. Results

As the shock front passes through the bubbles and voids, defects such as dislocations are generated. Indeed, the current study does show the nucleation and evolution of dislocations from this process as illustrated in Figure 2 regardless of bubble size or pressure. However, the type and density of dislocations is altered by these variables. Voids that are 2 nm in radius completely collapse at a particle velocity of 1.0 km/s, demonstrated in Figure 2. Note that the image shows the sample sliced through the middle to better view the defects generated at the surface of the

voids, though analysis to obtain dislocation density is performed on the entire 3D region. This image shows that the generated dislocations are primarily Shockley partials, shown as green lines, and stacking faults, shown as red lines. There are also some regions that can be construed as amorphous, indicated by yellow and purple atoms due to a loss of order in the crystalline structure around the voids. In contrast to the void, the 2 nm Cu-He-1.35 and Cu-He-2.39 do not fully collapse at 1.0 km/s. Specifically, as the shock passes through Cu-He-1.35, the bubble acquires a cuboidal shape as a result of dislocations being emitted in an anisotropic manner along the $\langle 111 \rangle$ planes. The effect is dramatic, if one considers that the internal pressures (1.35 and 2.39 GPa) are a small fraction of the applied shock stress (48, 123, and 170 GPa). The traces of the dislocations in the cross-sections of Figure 2 show the emission of dislocations, especially at the early stages of compression (18 ps). As the number of dislocations emitted increases, the dislocation network increases in complexity as the defects interact with one another. Molecular dynamics provides a detailed description of the dislocations generated, and discerns between perfect, partial, stair-rod, Hirth, and Frank dislocations. The majority of dislocations are configured as shear dislocation loops, which has been observed in previous MD simulations [53], [62], [70].

The quantification of the dislocations surrounding the voids for the three cases shown in Figure 2 reveals interesting features and trends. The dislocation density as a function of void size has been determined for voids subjected to a particle velocity of 1.0 km/s once the shock front reaches the rear surface of the sample at 21.0 ps, with detailed measurements of dislocation type included. For small voids (with a radius $R=2$ nm), Figure 3a shows that He-filled voids tend to generate more dislocations. Cu-He-1.35 generates the most dislocations at this small size, the majority of which are Shockley partial dislocations, as shown in Figure 3c; Cu-He-2.39 generates more perfect and sessile dislocations, detailed in Figures 3b and 3d. Though later calculations show an increase in

the critical stress required for dislocation nucleation as the internal pressure of a cavity increases, seemingly contradicting the number of dislocations, a void with a radius of 2.0 nm undergoes full and rapid collapse, which lessens the localization of dislocation production since there are no longer any vacancies available to be carried away by dislocation loops. Overall, the total dislocation density increases as a function of defect radius in all three cases. As illustrated in Figure 3b, the density of perfect dislocations decreases between radii of 2 nm and 3 nm, most clearly for the empty and the most densely filled void. As the size of the voids increases, prior to local melting, the total dislocation density tends to increase, similar to trends observed in past studies.

This behavior can be further examined by using a model first postulated by Lubarda et al. [54], that described the mechanism by which shear dislocation loops are generated and move to increase the volume of voids as verified in several molecular dynamics studies [46], [48], [62], [70], and also applies, *mutatis mutandis*, to the collapse of voids. This mechanism is especially relevant to the growth and collapse of voids with dimensions in the nanometer scale, before a highly work-hardened layer is formed surrounding the void. The essential features are shown as a hypothetical and simplified two-dimensional rendition in Figure 4. In order to remove the complexity of three-dimensional loading, the hydrostatic stress state is replaced by one in which compression in the X_1X_2 plane is symmetrically convergent (pseudo-hydrostatic) for the sake of simplifying the discussion. In general, to estimate which slip planes would activate for a given loading condition, a critical resolved shear stress along those planes is required, which can be estimated based on the Schmid Factor. For the bi-axial loading condition, only two slip planes, (111) and ($\bar{1}\bar{1}1$), will have the maximum Schmid factor and hence the ability to potentially activate. The stress state at the void surface is altered because normal stresses perpendicular to the surface are assumed to be zero. There are four positions, in Figure 4, where shear stresses are

maximum: they correspond to the point where the angle formed by the intersection of $(111)/(1\bar{1}1)$ planes at the void surface meets the tangent forming a 45° angle. Once the shear stress along this direction reaches a critical level, edge dislocations are emitted into the material, reducing the volume of the void. This is shown in a simplified manner in Figure 4 with the emission of two dislocations at each intersection; though Figure 4 is only two dimensional, the edge dislocations generated contribute to the formation of shear loops, which is addressed below.

In contrast to the above model, a closer look in 3D at the dislocations and stacking faults emitted from voids and helium bubbles via MD simulations (Figure 5), shows a complex deformation pattern which suggests that instead of just two, all four slip systems $((111), (11\bar{1}), (\bar{1}11)$ and $(1\bar{1}1))$ are simultaneously activated. While critical resolved shear stress calculations can provide an estimate of which slip systems might activate, it is important to note that the initial estimate is based on an average loading stress and does not take local stress concentrations into account [93]. These local stress concentrations are significant around the voids and bubbles, leading to the emission of shear dislocation loops as the defect is compressed. Importantly, the shear loops associated with changes in defect volume are special because they remain attached to the void/bubble surface, as discussed in previous works [54], [70]. While prior studies postulated the formation of prismatic loops (which were observed in BCC metals and demonstrated separation from the void surface) [70], no prismatic loops are observed in Figure 4 or in copper due to the separation of partial dislocations which impedes cross slip and prohibits prismatic loop generation.

A more realistic depiction of the mechanism of shear loop generation, propagation, and interaction than the one shown in Figure 4 is shown in Figure 6. Four planes of the $\{111\}$ family are shown, positioned such that they intersect the spherical void forming 45° angles, where shear

stresses are at their maximum. These planes bisect the diametral circles and the sphere apex. The intersections of these planes are the directions $[110]$, $[10\bar{1}]$, $[101]$, and $[\bar{1}\bar{1}0]$. Shockley partials are emitted when the shear stress on these planes reaches a critical level. The leading partials from different slip planes eventually intersect and create a network of reaction products that have been analyzed by Traiviratana et al. [53]. The intersection directions are shown in Figure 5 and can be identified as stair-rod dislocations, consistent with observations by Traiviratana et al [53]. While the process of shear loop generation under shock compression for a single void aligns with previous findings for void growth via shear loop emission, helium bubbles clearly diminish the number of dislocations, alluding to an increased resistance to deformation from the defect.

4. Discussion

The shear stress required to emit dislocation loops from the void/bubble surface (and thus initiate to process of collapse) is related to the shock stress, the void/bubble radius, and the internal pressure of the bubble. Three factors need to be considered: the global shear stress generated by the shock; the stress amplification produced at the void/bubble surface by the global stresses; and the temperature-dependent internal pressure in the bubble. These factors are idealized in Figure 7a. We assume, in accordance with Tang et al. [70], that the critical shear stress for dislocation emission, τ_c , is a function of the spherical bubble/void radius only, and do not consider variations in shock heating of the bulk copper. The maximum global shear stress, τ_{sg} , is expressed as follows for shock compression when the shock direction is along the y-direction:

$$\tau_{sg} = \frac{|\sigma_{yy} + \sigma_{xx}|}{2} = \frac{|\sigma_{yy} + \sigma_{zz}|}{2} \quad (1)$$

σ_{yy} , σ_{xx} , and σ_{zz} are the three components of stress generated by the propagation of a shock pulse along the y-direction. The uniaxial strain condition sets $\sigma_{zz} = \sigma_{xx}$. It is important to note that while there might be small differences between σ_{zz} and σ_{xx} due to differences in crystallographic

orientation, the assumption above generally applies for uniaxial strain loading. These lateral stresses are related to the shock stress, σ_{yy} , through:

$$\sigma_{zz} = \sigma_{xx} = \frac{\nu}{1-\nu} \sigma_{yy} \quad (2)$$

where ν is the Poisson's ratio. Thus:

$$\tau_{sg} = \frac{1-2\nu}{2(1-\nu)} \sigma_{yy} \quad (3)$$

At the surface of either a void or bubble, stress is concentrated due the presence of the defect. Assuming an isotropic material, the local shear stress at the surface of the spherical void/bubble, τ_{sl} is obtained from the classic stress concentration equation by Timoshenko and Goodier [94], similar to the procedure followed by Tang et al. [70]:

$$\tau_{sl} = \left[1 + \frac{13-5\nu}{2(7-5\nu)} \right] \tau_{sg} \quad (4)$$

When there is an internal pressure inside of the defect, such as the helium bubbles being explored in this work, the internal pressure opposes the shear stress imposed by shock. The radial (σ_r) and hoop stresses (σ_θ , σ_ϕ) created by the internal pressure (P) and are equal to [95]:

$$\sigma_r = -P \left(\frac{R}{r} \right)^3 \quad (5)$$

$$\sigma_\theta = \sigma_\phi = \frac{1}{2} P \left(\frac{R}{r} \right)^3 \quad (6)$$

where R is the radius of the bubble and r is the radial distance from the center of the bubble. The shear stress due to the internal pressure is obtained from the radial and hoop stresses:

$$\tau_p = \frac{1}{2} \left[P \left(\frac{R}{r} \right)^3 - \frac{1}{2} P \left(\frac{R}{r} \right)^3 \right] = \frac{3}{4} P \left(\frac{R}{r} \right)^3 \quad (7)$$

For $r=R$, corresponding to the surface of the void, this simplifies to

$$\tau_p = \frac{3}{4}P \quad (8)$$

The critical shear stress for dislocation emission from the void surface was calculated by Tang et al. [70] for pure copper with empty voids based on a balance between image forces (the attraction of dislocations to the free surface of the void) and the expansion force on the semi-circular segment due to the shear stresses resulting from hydrostatic loading. The critical maximum shear stress, τ_c , stress for the emission of dislocations is a function of the void radius, R:

$$\tau_c = \frac{2\gamma}{\pi\rho b_p} + \frac{b_p(2-\nu)G}{4\pi(1-\nu)R_1} \ln\left(\frac{8mR_1}{e^2\rho b_p} + \frac{\gamma_{SF}}{Gb_p}\right) \quad (9)$$

R_1 is the radius of the dislocation loop, which is assumed to be half of the void radius R. The shear modulus of copper is taken to be $G = 44.7$ GPa for copper, while Poisson's ratio is $\nu = 0.34$. $b_p = \frac{a}{6}\langle 112 \rangle = 0.148$ nm is the Burgers vector of a partial dislocation, a is the lattice constant of copper, $\gamma = 1.239$ Jm⁻² is the surface energy, $\gamma_{SF} = 44.4$ Jm⁻² is the stacking-fault energy [70], m is an approximation of the image interaction between a semi-circular dislocation loop and a void (~ 2.2), and ρ is the material density (8.9 g/cm³) [70].

The critical shear stress at which dislocations are emitted is represented in Fig. 7a. Dislocation emission is affected by both the global shear stress and uniaxial compression generated under shock loading. In this case, because the dislocation density is shown to decrease with the addition of helium to a cavity, implying that dislocation emission is driven by compression of the material. The critical shear stress for dislocation emission takes the form:

$$\tau_c = \tau_{sl} - \tau_p \quad (10)$$

Therefore, the critical shock stress, $(\sigma_{yy})_c$ at which dislocations are emitted can be calculated by inserting Eqns. 3 and 8 into Eqn. 10:

$$(\sigma_{yy})_c = \frac{2(1-\nu)}{1-2\nu} \left[1 + \frac{13-5\nu}{2(7-5\nu)} \right]^{-1} (\tau_c + \tau_p) \quad (11)$$

Substituting Eqns. 8 and 10 into Eqn. 11:

$$(\sigma_{yy})_c = \frac{2(1-\nu)}{1-2\nu} \left[1 + \frac{13-5\nu}{2(7-5\nu)} \right]^{-1} \left[\frac{2\gamma}{\pi\rho b_p} + \frac{b_p(2-\nu)G}{4\pi(1-\nu)R_1} \ln \left(\frac{8mR_1}{e^2\rho b_p} + \frac{\gamma_{SF}}{Gb_p} \right) + \frac{3}{4}P \right] \quad (12)$$

The shock stress required for dislocation emission during shock-induced void growth from the surface of empty and helium filled bubbles is shown as dashed lines in Figure 7b. The effect of the internal bubble pressure is seen in a clear manner. The same figure shows MD simulation results for four diameters at 21.0 ps, when the shock front has fully reached the rear surface, just before the material begins to release; these are indicated by symbols corresponding to the three different initial pressures: 0, 1.35, and 2.39 GPa. The analytical solution assumes a global measurement of the shear stress within the material, but the open symbols, which represent the shear stress measured via MD within a local cubic region having side length 40.0 nm and centered around each cavity, show stronger agreement with analytical results in comparison to the globally measured shear stress from MD. Copper atoms located sufficiently far enough from the defect are not subjected to the additional work done at the cavity surface as dislocation loops are formed, so the full bulk global shear stress measurement is skewed by the size of the sample in comparison to the size of the cavity embedded in each simulation. The minimum radius of 2.0 nm used in this study provides a ratio R/b equal to approximately 13, which is marked on the plot. Both the analytical and MD calculations predict a decrease in the stress required for dislocation generation at the surface of the defects as the initial defect size increases. Both MD results and the analytical model show that the addition of helium requires increased stress for dislocation generation since the internal pressure works to oppose deformation via shock compression. It is remarkable to note that for Cu-He-2.39 with an initial radius of 2.0 nm, the critical stress for dislocation emission (and

thus the beginning of partial collapse under shock compression) from the helium bubble is $(\sigma_{yy})_c \sim 4.75$ GPa, which is more than four times the initial internal pressure generated by helium. This is addressed in the following section, and is likely due to the increase in pressure as the helium bubble collapses, which increases the resistance to further deformation. The presence of helium bubbles generates a back pressure which opposes deformation and increases the stress needed to generate dislocations in comparison to empty voids.

Wilkerson and Ramesh [66], [67] and later Nitol et al. [71] present the effect of initial void radius on the stress required for the emission of dislocations in magnesium and find, as expected, a significant reduction in this stress, which they equate to the spall strength, with the increase in the void radius. They present the results of both MD calculations and an analytical solution. Importantly, they find that porosity has a significant effect on this stress, especially for pores with a radius larger than 3 nm (Fig. 9 of Nitol et al. [71]). Their analysis applies to our case, with a change in sign: the stress is tensile in their case and compressive in our case. We therefore compare their predictions with ours in Figure 7. Our analysis does not incorporate the effect of porosity and therefore the comparison is useful. The Wilkerson-Ramesh expression (Eq. 7 from Nitol et al. [71]) with the parameters converted to our symbols, takes the form:

$$(\sigma_{yy})_c = \left[\frac{Gb(R+1.3b\sqrt{2})^2}{4 \times 1.3\pi Rb(1-\nu)(R+1.3b/\sqrt{2})} + \frac{(\gamma+P)}{R} \right] \left(\frac{1-p}{1-p+\frac{3}{2}p^{2/3}} \right) \quad (13)$$

where the porosity defined as the ratio of the volume of the void by the volume of a cell containing it with dimensions l_x , l_y , and l_z :

$$p = \frac{\frac{4}{3}\pi R^3}{l_x l_y l_z} \quad (14)$$

In the limit where l_x , l_y , and l_z are infinite, $p=0$. Inspection of Eq. 13 shows that the critical stress for dislocation emission decreases with increasing porosity similar to our observation. The effect of the bubble pressure, P , can be added to the Wilkerson-Ramesh equation through the term $(\gamma+P)/R$. Figure 7c shows the predictions from the Wilkerson-Ramesh equation for different values of the porosity, which we made equal to those used by Nitol et al. [71]. The following parameters were used, for copper: The shear modulus of copper is taken to be $G = 44.7$ GPa, while Poisson's ratio is $\nu = 0.34$. $b = \frac{a}{6}\langle 112 \rangle = 0.148$ nm is the Burgers vector of a partial dislocation, a is the lattice constant of copper, $\gamma = 1.239$ Jm⁻² is the surface energy, $\gamma_{SF} = 44.4$ Jm⁻² is the stacking-fault energy [70], and $w_{alloy} = 1.3b$ as recommended by Nitol, et al [71]. We also use the same porosity parameters as Nitol, et al [71], which are each plotted in Figure 7c. It can be seen that the stresses are higher than the ones predicted by the Tang et al. [70] equation. This is due to the different assumptions involved in the generation of shear loops. The Wilkerson-Ramesh equation considers only the increase in surface energy, whereas the Tang equation is based on the emission of a semicircular dislocation loop from the void, the former having a radius equal to half the void radius.

4.1 Defect temperature & pressure effects

As the shock front moves through the material, the volume of the defect decreases, leading to an increase in temperature and pressure for helium-filled defects. For empty voids, local hot spots on the void surface are manifested instead. The initial defect size and internal pressure each factor in to the shock behavior since the generation of dislocations is affected by both parameters. In Figure 3, helium-filled defects produced the most dislocations in comparison to voids with a radius

of 2.0 nm despite helium-filled defects requiring a higher critical stress for dislocation emission. Though we expect the void to produce more dislocations since it requires less stress to emit dislocations, illustrated by Figure 7b, the void is rapidly compressed and converted to a localized plastic region, shown in Figures 2a-c. The void collapses so rapidly that it cannot serve as a source of dislocations long enough to exceed the dislocation production of the helium bubbles of the same size. Li, et al. observed a similar trend, where the collapse and deformation of both voids and helium bubbles is constrained for radii less than 2.0 nm [80]. Aside from this exception, voids produce the most dislocations since they have no back pressure to resist the shock front.

The total plasticity around a void or bubble can be affected by the temperature rise associated with the collapse of the bubble. Figure 8 illustrates the associated local temperature profile for the voids/bubbles with an initial radius of 9.0 nm after shock loading for an internal cross section of the material. While prior discussion focused on smaller voids and helium bubbles, the case of defects with an initial radius of 9.0 nm better depicts the formation of hot spots as the material undergoes compression. At 1 km/s, none of the larger 9 nm defects are fully collapsed, though a highly localized hot spot is formed around the empty void. At this particle velocity and defect size, the voids are able to easily produce more dislocations since the stress required to produce dislocations is less for voids as compared to helium bubbles. Adding helium prevents the complete collapse of the helium bubble in Cu-He-1.35; as the material is compressed, the temperature increase is concentrated throughout the helium defect. This effect is pronounced in Cu-He-2.39; while the material certainly generates a hot spot, the addition of helium causes the local heat to be more dispersed through the material. Though this means the temperature is slightly lower when comparing empty voids to helium bubbles, the temperature increase is spread throughout the material local to the defects, illustrated in Figure 8.

Shock compression decreases the volume of voids and bubbles in all cases; for Cu-He-1.35 and Cu-He-2.39, this generates an increase in the temperature and pressure within the defect, which becomes more pronounced as the shock increases in strength. Temperature and pressure of the helium bubbles are calculated directly from our simulations in the subsequent discussion. Figure 9a shows temperature of the helium bubble as a function of particle velocity for initial defect radii of 2.0 and 9.0 nm in both Cu-He-1.35 and Cu-He-2.39. While the clear increase in temperature as a function of particle velocity is not surprising, it is interesting to note that smaller defects and Cu-He-2.39 tend to be closer in temperature while Cu-He-1.35 with an initial bubble radius of 9.0 nm is significantly hotter than the other cases. The internal pressure of helium bubbles, which remain intact throughout all simulations performed in this study, display an order of magnitude increase as a function of particle velocity. Taken together, the increase in defect temperature and pressure combined with the resistance to shear loop generation by the helium bubbles demonstrates that the defect resists deformation due to the back pressure within the bubble.

5 Conclusions

Simulations of shock compression on single crystal copper with pre-existing voids, both empty and helium-filled, along the [111] directions were performed at different stresses in order to better understand the atomistic scale mechanisms of void collapse during shock loading. The following significant conclusions are reached:

- The distribution and densities of dislocations generated are quantified from MD simulations for different void sizes, pressures, and void radii and the differences obtained are interpreted in terms of the mechanisms of dislocation emission.

- The mechanism of void collapse by the emission of dislocations is established and is found to be similar to the earlier mechanism postulated by Lubarda et al.[54] and modeled using MD by Traiviratana et al.[53] and Tang et al. [70] for void growth in FCC metals.
- The emission of dislocation proceeds by the formation, first, of a leading partial dislocation, the formation of a stacking fault, and the emission of a trailing dislocation. The dislocations on different $\{111\}$ planes react and form sessile dislocations and a complex network of work hardened material.
- As the particle velocity is increased to 2.0 and 2.5 km/s, increasing dislocation densities and eventually locally melted regions are observed due to the formation of hot spots adjacent to both He-filled and empty voids.
- There are significant differences between the threshold shock stress for the emission of dislocations and associated void collapse between empty and helium-filled voids, the latter resisting collapse more effectively than the former.
- The threshold stress for the emission of dislocations is calculated as a function of void radius by both analytical and computational means and a clear trend of decreasing stress with increasing radius is observed. Additionally, the critical shock stress for emission of dislocations around helium filled bubbles is higher than that of empty voids.

Acknowledgements

Molecular dynamics simulations utilized resources were provided by the LANL Institutional Computing Program and funding was provided by the Science Campaigns. The support provided to Rachel Flanagan and Marc Meyers by the Center for Matter in Extreme Conditions (award number DE-NA0003842) is gratefully acknowledged. This work was supported by the U.S. Department of Energy (DOE) through the Los Alamos National Laboratory. The Los Alamos National Laboratory is operated by Triad National Security, LLC, for the National Nuclear Security Administration of the U.S. Department of Energy (Contract No. 89233218CNA000001).

Data Availability

The data that support the findings of this study are available from the corresponding author upon reasonable request.

Author Contributions

RMF, MAM, and SJF proposed the project. RMF prepared the manuscript and figures. RMF performed the simulations which were evaluated by RMF, MAM, SMV, and SJF. All authors contributed to discussions of the paper.

Competing Interests

The Authors declare no Competing Financial or Non-Financial Interests.

References

- [1] D. R. Curran, L. Seaman, and D. A. Shockey, “Dynamic failure of solids,” *Physics Reports*, vol. 147, no. 5, pp. 253–388, Mar. 1987, doi: 10.1016/0370-1573(87)90049-4.
- [2] M. A. Meyers and C. Taylor Aimone, “Dynamic fracture (spalling) of metals,” *Progress in Materials Science*, vol. 28, no. 1, pp. 1–96, Jan. 1983, doi: 10.1016/0079-6425(83)90003-8.
- [3] R. W. Minich, J. U. Cazamias, M. Kumar, and A. J. Schwartz, “Effect of microstructural length scales on spall behavior of copper,” *Metall and Mat Trans A*, vol. 35, no. 9, pp. 2663–2673, Sep. 2004, doi: 10.1007/s11661-004-0212-7.
- [4] R. W. Minich, M. Kumar, A. Schwarz, and J. Cazamias, “Scaling, Microstructure and Dynamic Fracture,” *AIP Conference Proceedings*, vol. 845, no. 1, pp. 642–645, Jul. 2006, doi: 10.1063/1.2263404.
- [5] N. K. Bourne, J. C. F. Millett, and G. T. Gray, “On the shock compression of polycrystalline metals,” *J Mater Sci*, vol. 44, no. 13, pp. 3319–3343, Jul. 2009, doi: 10.1007/s10853-009-3394-y.
- [6] “High-Strain-Rate Deformation: Mechanical Behavior and Deformation Substructures Induced | Annual Review of Materials Research.”
<https://www.annualreviews.org/doi/abs/10.1146/annurev-matsci-070511-155034> (accessed Jul. 14, 2020).
- [7] E. N. Hahn and S. J. Fensin, “Influence of defects on the shock Hugoniot of tantalum,” *Journal of Applied Physics*, vol. 125, no. 21, p. 215902, Jun. 2019, doi: 10.1063/1.5096526.
- [8] J. N. Florando, N. R. Barton, B. S. El-Dasher, J. M. McNaney, and M. Kumar, “Analysis of deformation twinning in tantalum single crystals under shock loading conditions,” *Journal of Applied Physics*, vol. 113, no. 8, p. 083522, Feb. 2013, doi: 10.1063/1.4792227.

- [9] J. C. F. Millett, G. Whiteman, N. T. Park, S. Case, and N. K. Bourne, “The role of cold work on the shock response of tantalum,” *Journal of Applied Physics*, vol. 113, no. 23, p. 233502, Jun. 2013, doi: 10.1063/1.4810896.
- [10] S.-N. Luo, T. C. Germann, and D. L. Tonks, “The effect of vacancies on dynamic response of single crystal Cu to shock waves,” *Journal of Applied Physics*, vol. 107, no. 5, p. 056102, Mar. 2010, doi: 10.1063/1.3326941.
- [11] T. Qiu, Y. Xiong, S. Xiao, X. Li, W. Hu, and H. Deng, “Non-equilibrium molecular dynamics simulations of the spallation in Ni: Effect of vacancies,” *Computational Materials Science*, vol. 137, pp. 273–281, Sep. 2017, doi: 10.1016/j.commatsci.2017.05.039.
- [12] E. Lin, H. Shi, and L. Niu, “Effects of orientation and vacancy defects on the shock Hugoniot behavior and spallation of single-crystal copper,” *Modelling Simul. Mater. Sci. Eng.*, vol. 22, no. 3, p. 035012, Mar. 2014, doi: 10.1088/0965-0393/22/3/035012.
- [13] E. B. Zaretsky and G. I. Kanel, “Yield stress, polymorphic transformation, and spall fracture of shock-loaded iron in various structural states and at various temperatures,” *Journal of Applied Physics*, vol. 117, no. 19, p. 195901, May 2015, doi: 10.1063/1.4921356.
- [14] D. R. Jones, B. M. Morrow, C. P. Trujillo, G. T. Gray, and E. K. Cerreta, “The α - ω phase transition in shock-loaded titanium,” *Journal of Applied Physics*, vol. 122, no. 4, p. 045902, Jul. 2017, doi: 10.1063/1.4987146.
- [15] T. de Ressaiguier and M. Hallouin, “Effects of the α - ϵ phase transition on wave propagation and spallation in laser shock-loaded iron,” *Phys. Rev. B*, vol. 77, no. 17, p. 174107, May 2008, doi: 10.1103/PhysRevB.77.174107.

- [16] N. Amadou, T. de Resseguier, A. Dragon, and E. Brambrink, “Coupling between plasticity and phase transition in shock- and ramp-compressed single-crystal iron,” *Phys. Rev. B*, vol. 98, no. 2, p. 024104, Jul. 2018, doi: 10.1103/PhysRevB.98.024104.
- [17] K. Mackenchery, R. R. Valisetty, R. R. Namburu, A. Stukowski, A. M. Rajendran, and A. M. Dongare, “Dislocation evolution and peak spall strengths in single crystal and nanocrystalline Cu,” *Journal of Applied Physics*, vol. 119, no. 4, p. 044301, Jan. 2016, doi: 10.1063/1.4939867.
- [18] E. N. Hahn and M. A. Meyers, “Grain-size dependent mechanical behavior of nanocrystalline metals,” *Materials Science and Engineering: A*, vol. 646, pp. 101–134, Oct. 2015, doi: 10.1016/j.msea.2015.07.075.
- [19] T. P. Remington *et al.*, “Spall strength dependence on grain size and strain rate in tantalum,” *Acta Materialia*, vol. 158, pp. 313–329, Oct. 2018, doi: 10.1016/j.actamat.2018.07.048.
- [20] E. N. Hahn, T. C. Germann, R. Ravelo, J. E. Hammerberg, and M. A. Meyers, “On the ultimate tensile strength of tantalum,” *Acta Materialia*, vol. 126, pp. 313–328, Mar. 2017, doi: 10.1016/j.actamat.2016.12.033.
- [21] G. T. (Rusty) Gray, “High-Strain-Rate Deformation: Mechanical Behavior and Deformation Substructures Induced,” *Annual Review of Materials Research*, vol. 42, no. 1, pp. 285–303, 2012, doi: 10.1146/annurev-matsci-070511-155034.
- [22] M. A. Meyers, A. Mishra, and D. J. Benson, “Mechanical properties of nanocrystalline materials,” *Progress in Materials Science*, vol. 51, no. 4, pp. 427–556, May 2006, doi: 10.1016/j.pmatsci.2005.08.003.

- [23] J. Schiøtz and K. W. Jacobsen, “A Maximum in the Strength of Nanocrystalline Copper,” *Science*, vol. 301, no. 5638, pp. 1357–1359, Sep. 2003, doi: 10.1126/science.1086636.
- [24] E. M. Bringa *et al.*, “Ultrahigh Strength in Nanocrystalline Materials Under Shock Loading,” *Science*, vol. 309, no. 5742, pp. 1838–1841, Sep. 2005, doi: 10.1126/science.1116723.
- [25] S.-N. Luo, T. C. Germann, T. G. Desai, D. L. Tonks, and Q. An, “Anisotropic shock response of columnar nanocrystalline Cu,” *Journal of Applied Physics*, vol. 107, no. 12, p. 123507, Jun. 2010, doi: 10.1063/1.3437654.
- [26] A. M. Dongare, A. M. Rajendran, B. LaMattina, M. A. Zikry, and D. W. Brenner, “Atomic scale studies of spall behavior in nanocrystalline Cu,” *Journal of Applied Physics*, vol. 108, no. 11, p. 113518, Dec. 2010, doi: 10.1063/1.3517827.
- [27] A. M. Dongare, A. M. Rajendran, B. LaMattina, M. A. Zikry, and D. W. Brenner, “Atomic scale simulations of ductile failure micromechanisms in nanocrystalline Cu at high strain rates,” *Phys. Rev. B*, vol. 80, no. 10, p. 104108, Sep. 2009, doi: 10.1103/PhysRevB.80.104108.
- [28] C. H. Lu *et al.*, “Laser compression of nanocrystalline tantalum,” *Acta Materialia*, vol. 61, no. 20, pp. 7767–7780, Dec. 2013, doi: 10.1016/j.actamat.2013.09.016.
- [29] Y. T. Zhu, X. Z. Liao, and X. L. Wu, “Deformation twinning in nanocrystalline materials,” *Progress in Materials Science*, vol. 57, no. 1, pp. 1–62, Jan. 2012, doi: 10.1016/j.pmatsci.2011.05.001.
- [30] S. J. Fensin, E. K. Cerreta, G. T. G. Iii, and S. M. Valone, “Why are some Interfaces in Materials Stronger than others?,” *Scientific Reports*, vol. 4, no. 1, Art. no. 1, Jun. 2014, doi: 10.1038/srep05461.

- [31] S. J. Fensin, S. M. Valone, E. K. Cerreta, and G. T. Gray, "Influence of grain boundary properties on spall strength: Grain boundary energy and excess volume," *Journal of Applied Physics*, vol. 112, no. 8, p. 083529, Oct. 2012, doi: 10.1063/1.4761816.
- [32] M. A. Meyers and M. S. Carvalho, "Shock-front irregularities in polycrystalline metals," *Materials Science and Engineering*, vol. 24, no. 1, pp. 131–135, Jul. 1976, doi: 10.1016/0025-5416(76)90102-6.
- [33] J. P. Escobedo, E. K. Cerreta, and D. Dennis-Koller, "Effect of Crystalline Structure on Intergranular Failure During Shock Loading," *JOM*, vol. 66, no. 1, pp. 156–164, Jan. 2014, doi: 10.1007/s11837-013-0798-6.
- [34] E. M. Bringa, S. Traiviratana, and M. A. Meyers, "Void initiation in fcc metals: Effect of loading orientation and nanocrystalline effects," *Acta Materialia*, vol. 58, no. 13, pp. 4458–4477, Aug. 2010, doi: 10.1016/j.actamat.2010.04.043.
- [35] D. D. Mallick, C. L. Williams, and J. W. Wilkerson, "A Brief Review of Spall Failure in Pure and Alloyed Magnesium," *J. dynamic behavior mater.*, Jan. 2020, doi: 10.1007/s40870-020-00233-z.
- [36] R. S. Hixson, J. N. Johnson, G. T. Gray, and J. D. Price, "Effects of interfacial bonding on spallation in metal-matrix composites," *AIP Conference Proceedings*, vol. 370, no. 1, pp. 555–558, May 1996, doi: 10.1063/1.50872.
- [37] S. V. Razorenov, G. I. Kanel, B. Herrmann, E. B. Zaretsky, and G. E. Ivanchihina, "Influence of nano- size inclusions on spall fracture of copper single crystals," *AIP Conference Proceedings*, vol. 955, no. 1, pp. 581–584, Dec. 2007, doi: 10.1063/1.2833154.

- [38] X. Chen, J. R. Asay, S. K. Dwivedi, and D. P. Field, “Spall behavior of aluminum with varying microstructures,” *Journal of Applied Physics*, vol. 99, no. 2, p. 023528, Jan. 2006, doi: 10.1063/1.2165409.
- [39] S. J. Fensin, J. P. Escobedo, G. T. Gray, B. M. Patterson, C. P. Trujillo, and E. K. Cerreta, “Dynamic damage nucleation and evolution in multiphase materials,” *Journal of Applied Physics*, vol. 115, no. 20, p. 203516, May 2014, doi: 10.1063/1.4880435.
- [40] J. Chen, M. A. Tschopp, and A. M. Dongare, “Role of nanoscale Cu/Ta interfaces on the shock compression and spall failure of nanocrystalline Cu/Ta systems at the atomic scales,” *J Mater Sci*, vol. 53, no. 8, pp. 5745–5765, Apr. 2018, doi: 10.1007/s10853-017-1879-7.
- [41] L. Farbaniec, C. L. Williams, L. Kecskes, K. T. Ramesh, and R. Becker, “Microstructural effects on the spall properties of ECAE-processed AZ31B magnesium alloy,” *International Journal of Impact Engineering*, vol. 98, pp. 34–41, Dec. 2016, doi: 10.1016/j.ijimpeng.2016.08.001.
- [42] N. M. Krywopusk, C. L. Williams, L. J. Kecskes, and T. P. Weihs, “Characterization of spalled AZ31B processed by ECAE,” *Materials Science and Engineering: A*, vol. 767, p. 138298, Nov. 2019, doi: 10.1016/j.msea.2019.138298.
- [43] “The Role of Second Phase Intermetallic Particles on the Spall Failure of 5083 Aluminum | SpringerLink.” <https://link.springer.com/article/10.1007%2Fs40870-016-0082-2> (accessed Aug. 25, 2020).
- [44] J. C. Cheng *et al.*, “Effects of second-phase boron particles on impact response of aluminum,” *Materials Science and Engineering: A*, vol. 793, p. 139805, Aug. 2020, doi: 10.1016/j.msea.2020.139805.

- [45] T. Hatano, “Dislocation Nucleation in Shocked fcc Solids: Effects of Temperature and Preexisting Voids,” *Phys. Rev. Lett.*, vol. 93, no. 8, p. 085501, Aug. 2004, doi: 10.1103/PhysRevLett.93.085501.
- [46] T. Hatano, “Spatiotemporal Behavior of Void Collapse in Shocked Solids,” *Phys. Rev. Lett.*, vol. 92, no. 1, p. 015503, Jan. 2004, doi: 10.1103/PhysRevLett.92.015503.
- [47] B. L. Holian, T. C. Germann, J.-B. Maillet, and C. T. White, “Atomistic Mechanism for Hot Spot Initiation,” *Physical Review Letters*, vol. 89, no. 28, Dec. 2002, doi: 10.1103/PhysRevLett.89.285501.
- [48] J. W. Mintmire, D. H. Robertson, and C. T. White, “Molecular-dynamics simulations of void collapse in shocked model-molecular solids,” *Phys. Rev. B*, vol. 49, no. 21, pp. 14859–14864, Jun. 1994, doi: 10.1103/PhysRevB.49.14859.
- [49] D. H. Tsai and R. W. Armstrong, “Defect-Enhanced Structural Relaxation Mechanism for the Evolution of Hot Spots in Rapidly Compressed Crystals,” *J. Phys. Chem.*, vol. 98, no. 43, pp. 10997–11000, Oct. 1994, doi: 10.1021/j100094a001.
- [50] L. Phillips, R. S. Sinkovits, E. S. Oran, and J. P. Boris, “The interaction of shocks and defects in Lennard-Jones crystals,” *J. Phys.: Condens. Matter*, vol. 5, no. 35, pp. 6357–6376, Aug. 1993, doi: 10.1088/0953-8984/5/35/003.
- [51] A. Strachan, T. Çağın, and W. A. Goddard, “Critical behavior in spallation failure of metals,” *Phys. Rev. B*, vol. 63, no. 6, p. 060103, Jan. 2001, doi: 10.1103/PhysRevB.63.060103.
- [52] M. A. Meyers, S. Traiviratana, V. A. Lubarda, D. J. Benson, and E. M. Bringa, “The role of dislocations in the growth of nanosized voids in ductile failure of metals,” *JOM*, vol. 61, no. 2, p. 35, Feb. 2009, doi: 10.1007/s11837-009-0025-7.

- [53] S. Traiviratana, E. M. Bringa, D. J. Benson, and M. A. Meyers, “Void growth in metals: Atomistic calculations,” *Acta Materialia*, vol. 56, no. 15, pp. 3874–3886, Sep. 2008, doi: 10.1016/j.actamat.2008.03.047.
- [54] V. A. Lubarda, M. S. Schneider, D. H. Kalantar, B. A. Remington, and M. A. Meyers, “Void growth by dislocation emission,” *Acta Materialia*, vol. 52, no. 6, pp. 1397–1408, Apr. 2004, doi: 10.1016/j.actamat.2003.11.022.
- [55] K. J. Zhao, C. Q. Chen, Y. P. Shen, and T. J. Lu, “Molecular dynamics study on the nano-void growth in face-centered cubic single crystal copper,” *Computational Materials Science*, vol. 46, no. 3, pp. 749–754, Sep. 2009, doi: 10.1016/j.commatsci.2009.04.034.
- [56] D. Tramontina *et al.*, “Molecular dynamics simulations of shock-induced plasticity in tantalum,” *High Energy Density Physics*, vol. 10, pp. 9–15, Mar. 2014, doi: 10.1016/j.hedp.2013.10.007.
- [57] E. Dekel, S. Eliezer, Z. Henis, E. Moshe, A. Ludmirsky, and I. B. Goldberg, “Spallation model for the high strain rates range,” *Journal of Applied Physics*, vol. 84, no. 9, pp. 4851–4858, Oct. 1998, doi: 10.1063/1.368727.
- [58] J. Belak, “On the nucleation and growth of voids at high strain-rates,” *Journal of Computer-Aided Materials Design*, vol. 5, no. 2, pp. 193–206, May 1998, doi: 10.1023/A:1008685029849.
- [59] E. T. Seppälä, J. Belak, and R. E. Rudd, “Effect of stress triaxiality on void growth in dynamic fracture of metals: A molecular dynamics study,” *Phys. Rev. B*, vol. 69, no. 13, p. 134101, Apr. 2004, doi: 10.1103/PhysRevB.69.134101.

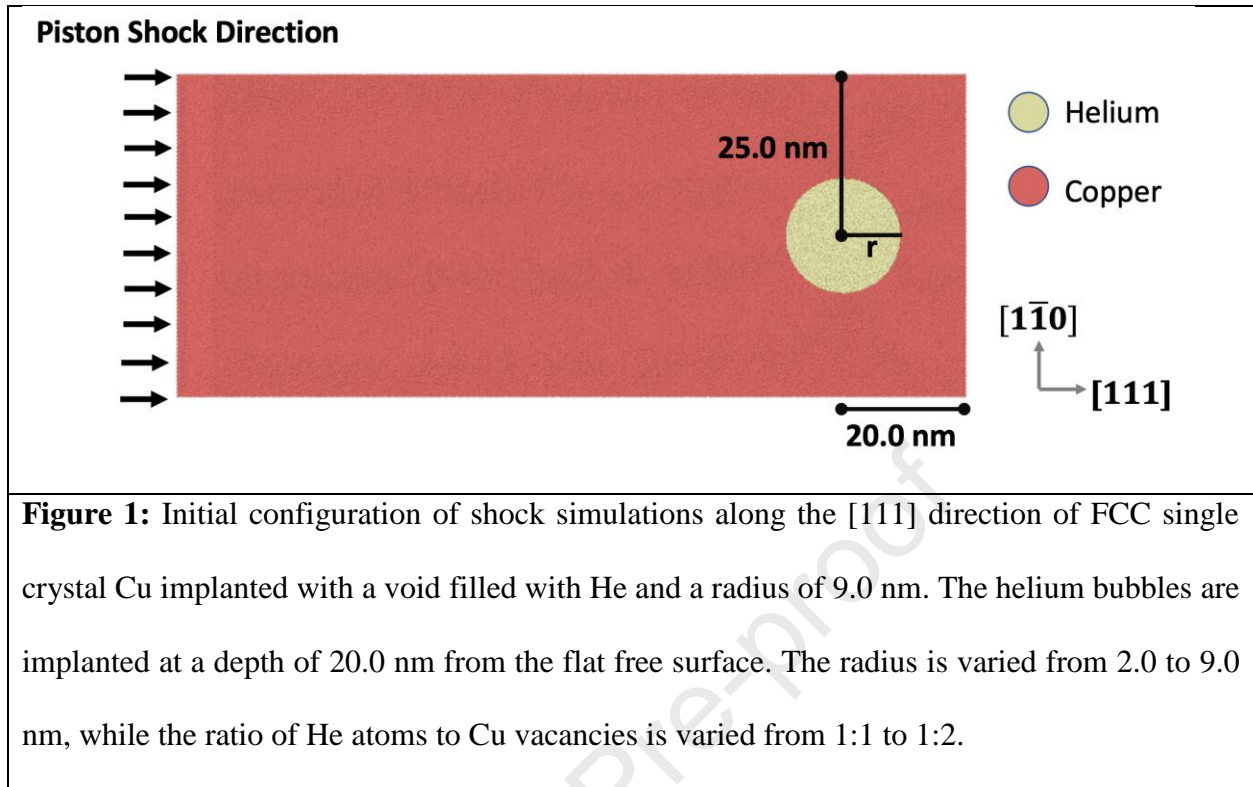
- [60] W. Herrmann, “Constitutive Equation for the Dynamic Compaction of Ductile Porous Materials,” *Journal of Applied Physics*, vol. 40, no. 6, pp. 2490–2499, May 1969, doi: 10.1063/1.1658021.
- [61] M. M. Carroll and A. C. Holt, “Steady waves in ductile porous solids,” *Journal of Applied Physics*, vol. 44, no. 10, pp. 4388–4392, Oct. 1973, doi: 10.1063/1.1661970.
- [62] L. P. Dávila *et al.*, “Atomistic modeling of shock-induced void collapse in copper,” *Appl. Phys. Lett.*, vol. 86, no. 16, p. 161902, Apr. 2005, doi: 10.1063/1.1906307.
- [63] P. Erhart, E. M. Bringa, M. Kumar, and K. Albe, “Atomistic mechanism of shock-induced void collapse in nanoporous metals,” *Phys. Rev. B*, vol. 72, no. 5, p. 052104, Aug. 2005, doi: 10.1103/PhysRevB.72.052104.
- [64] C. J. Ruestes *et al.*, “Atomistic simulation of the mechanical response of a nanoporous body-centered cubic metal,” *Scripta Materialia*, vol. 68, no. 10, pp. 817–820, May 2013, doi: 10.1016/j.scriptamat.2013.01.035.
- [65] C. J. Ruestes, E. M. Bringa, A. Stukowski, J. F. Rodríguez Nieva, Y. Tang, and M. A. Meyers, “Plastic deformation of a porous bcc metal containing nanometer sized voids,” *Computational Materials Science*, vol. 88, pp. 92–102, Jun. 2014, doi: 10.1016/j.commatsci.2014.02.047.
- [66] J. W. Wilkerson and K. T. Ramesh, “A dynamic void growth model governed by dislocation kinetics,” *Journal of the Mechanics and Physics of Solids*, vol. 70, pp. 262–280, Oct. 2014, doi: 10.1016/j.jmps.2014.05.018.
- [67] J. W. Wilkerson and K. T. Ramesh, “A closed-form criterion for dislocation emission in nano-porous materials under arbitrary thermomechanical loading,” *Journal of the Mechanics and Physics of Solids*, vol. 86, pp. 94–116, Jan. 2016, doi: 10.1016/j.jmps.2015.10.005.

- [68] V. A. Lubarda, “Emission of dislocations from nanovoids under combined loading,” *International Journal of Plasticity*, vol. 27, no. 2, pp. 181–200, Feb. 2011, doi: 10.1016/j.ijplas.2010.04.005.
- [69] V. A. Lubarda, “Image force on a straight dislocation emitted from a cylindrical void,” *International Journal of Solids and Structures*, vol. 48, no. 5, pp. 648–660, Mar. 2011, doi: 10.1016/j.ijsolstr.2010.11.006.
- [70] Y. Tang, E. M. Bringa, and M. A. Meyers, “Ductile tensile failure in metals through initiation and growth of nanosized voids,” *Acta Materialia*, vol. 60, no. 12, pp. 4856–4865, Jul. 2012, doi: 10.1016/j.actamat.2012.05.030.
- [71] M. S. Nitol, S. Adibi, C. D. Barrett, and J. W. Wilkerson, “Solid solution softening in dislocation-starved Mg–Al alloys,” *Mechanics of Materials*, vol. 150, p. 103588, Nov. 2020, doi: 10.1016/j.mechmat.2020.103588.
- [72] H. Trinkaus and B. N. Singh, “Helium accumulation in metals during irradiation – where do we stand?,” *Journal of Nuclear Materials*, vol. 323, no. 2–3, pp. 229–242, Dec. 2003, doi: 10.1016/j.jnucmat.2003.09.001.
- [73] T. Yamamoto, G. R. Odette, P. Miao, D. J. Edwards, and R. J. Kurtz, “Helium effects on microstructural evolution in tempered martensitic steels: In situ helium implanter studies in HFIR,” *Journal of Nuclear Materials*, vol. 386–388, pp. 338–341, Apr. 2009, doi: 10.1016/j.jnucmat.2008.12.134.
- [74] R. S. Barnes, G. B. Redding, and A. H. Cottrell, “The observation of vacancy sources in metals,” *Philosophical Magazine*, vol. 3, no. 25, pp. 97–99, Jan. 1958, doi: 10.1080/14786435808243230.

- [75] P. A. Thorsen, J. B. Bilde-Sørensen, and B. N. Singh, “Bubble formation at grain boundaries in helium implanted copper,” *Scripta Materialia*, vol. 51, no. 6, pp. 557–560, Sep. 2004, doi: 10.1016/j.scriptamat.2004.05.038.
- [76] R. S. Barnes, “Embrittlement of Stainless Steels and Nickel-Based Alloys at High Temperature Induced by Neutron Radiation | Nature.”
<https://www.nature.com/articles/2061307a0> (accessed Jun. 14, 2018).
- [77] V. Raineri, S. Coffa, E. Szilágyi, J. Gyulai, and E. Rimini, “He-vacancy interactions in Si and their influence on bubble formation and evolution,” *Physical Review B*, vol. 61, no. 2, pp. 937–945, Jan. 2000, doi: 10.1103/PhysRevB.61.937.
- [78] D. F. Cowgill, “Helium Nano-Bubble Evolution in Aging Metal Tritides,” *Fusion Science and Technology*, vol. 48, no. 1, pp. 539–544, Aug. 2005, doi: 10.13182/FST48-539.
- [79] L. Pizzagalli, M. L. David, and M. Bertolus, “Molecular dynamics simulation of the initial stages of He bubbles formation in silicon,” *Modelling and Simulation in Materials Science and Engineering*, vol. 21, no. 6, p. 065002, Sep. 2013, doi: 10.1088/0965-0393/21/6/065002.
- [80] B. Li, L. Wang, J. C. E. H. H. Ma, and S. N. Luo, “Shock response of He bubbles in single crystal Cu,” *Journal of Applied Physics*, vol. 116, no. 21, p. 213506, Dec. 2014, doi: 10.1063/1.4903732.
- [81] Q. Guo, P. Landau, P. Hosemann, Y. Wang, and J. R. Greer, “Helium Implantation Effects on the Compressive Response of Cu Nanopillars,” *Small*, vol. 9, no. 5, pp. 691–696, Mar. 2013, doi: 10.1002/sml.201201614.
- [82] B. Glam, M. Strauss, S. Eliezer, and D. Moreno, “Shock compression and spall formation in aluminum containing helium bubbles at room temperature and near the melting

- temperature: Experiments and simulations,” *International Journal of Impact Engineering*, vol. 65, pp. 1–12, Mar. 2014, doi: 10.1016/j.ijimpeng.2013.10.010.
- [83] H.-Y. Wang, X.-S. Li, W.-J. Zhu, X.-L. Deng, Z.-F. Song, and X.-R. Chen, “Atomistic modelling of the plastic deformation of helium bubbles and voids in aluminium under shock compression,” *Radiation Effects and Defects in Solids*, vol. 169, no. 2, pp. 109–116, Feb. 2014, doi: 10.1080/10420150.2013.848449.
- [84] M. B. Prime *et al.*, “Using growth and arrest of Richtmyer-Meshkov instabilities and Lagrangian simulations to study high-rate material strength,” *Journal of Physics: Conference Series*, vol. 500, no. 11, p. 112051, May 2014, doi: 10.1088/1742-6596/500/11/112051.
- [85] R. M. Flanagan, E. N. Hahn, T. C. Germann, M. A. Meyers, and S. J. Fensin, “Molecular dynamics simulations of ejecta formation in helium-implanted copper,” *Scripta Materialia*, vol. 178, pp. 114–118, Mar. 2020, doi: 10.1016/j.scriptamat.2019.11.005.
- [86] S. Fensin, D. Jones, D. Martinez, C. Lear, and J. Payton, “The Role of Helium on Ejecta Production in Copper,” *Materials*, vol. 13, no. 6, Art. no. 6, Jan. 2020, doi: 10.3390/ma13061270.
- [87] S. Plimpton, “Fast Parallel Algorithms for Short-Range Molecular Dynamics,” *Journal of Computational Physics*, vol. 117, no. 1, pp. 1–19, Mar. 1995, doi: 10.1006/jcph.1995.1039.
- [88] A. Kashinath and M. J. Demkowicz, “A predictive interatomic potential for He in Cu and Nb,” *Modelling Simul. Mater. Sci. Eng.*, vol. 19, no. 3, p. 035007, Mar. 2011, doi: 10.1088/0965-0393/19/3/035007.
- [89] R. L. Mills, D. H. Liebenberg, and J. C. Bronson, “Equation of state and melting properties of ${}^4\text{He}$ from measurements to 20 kbar,” *Phys. Rev. B*, vol. 21, no. 11, pp. 5137–5148, Jun. 1980, doi: 10.1103/PhysRevB.21.5137.

- [90] A. Stukowski, “Visualization and analysis of atomistic simulation data with OVITO—the Open Visualization Tool,” *Modelling Simul. Mater. Sci. Eng.*, vol. 18, no. 1, p. 015012, Dec. 2009, doi: 10.1088/0965-0393/18/1/015012.
- [91] B. L. Holian, “Plasticity Induced by Shock Waves in Nonequilibrium Molecular-Dynamics Simulations,” *Science*, vol. 280, no. 5372, pp. 2085–2088, Jun. 1998, doi: 10.1126/science.280.5372.2085.
- [92] A. Stukowski, V. V. Bulatov, and A. Arsenlis, “Automated identification and indexing of dislocations in crystal interfaces,” *Modelling Simul. Mater. Sci. Eng.*, vol. 20, no. 8, p. 085007, Oct. 2012, doi: 10.1088/0965-0393/20/8/085007.
- [93] S. J. Fensin, C. Brandl, E. K. Cerreta, G. T. Gray, T. C. Germann, and S. M. Valone, “Nanoscale Plasticity at Grain Boundaries in Face-centered Cubic Copper Under Shock Loading,” *JOM*, vol. 65, no. 3, pp. 410–418, Mar. 2013, doi: 10.1007/s11837-012-0546-3.
- [94] S. Timoshenko and J. N. Goodier, *Theory of Elasticity*. McGraw-Hill, 1951.
- [95] V. A. Lubarda and M. A. Meyers, “ON PLASTIC VOID GROWTH IN STRONG DUCTILE MATERIALS,” p. 22.



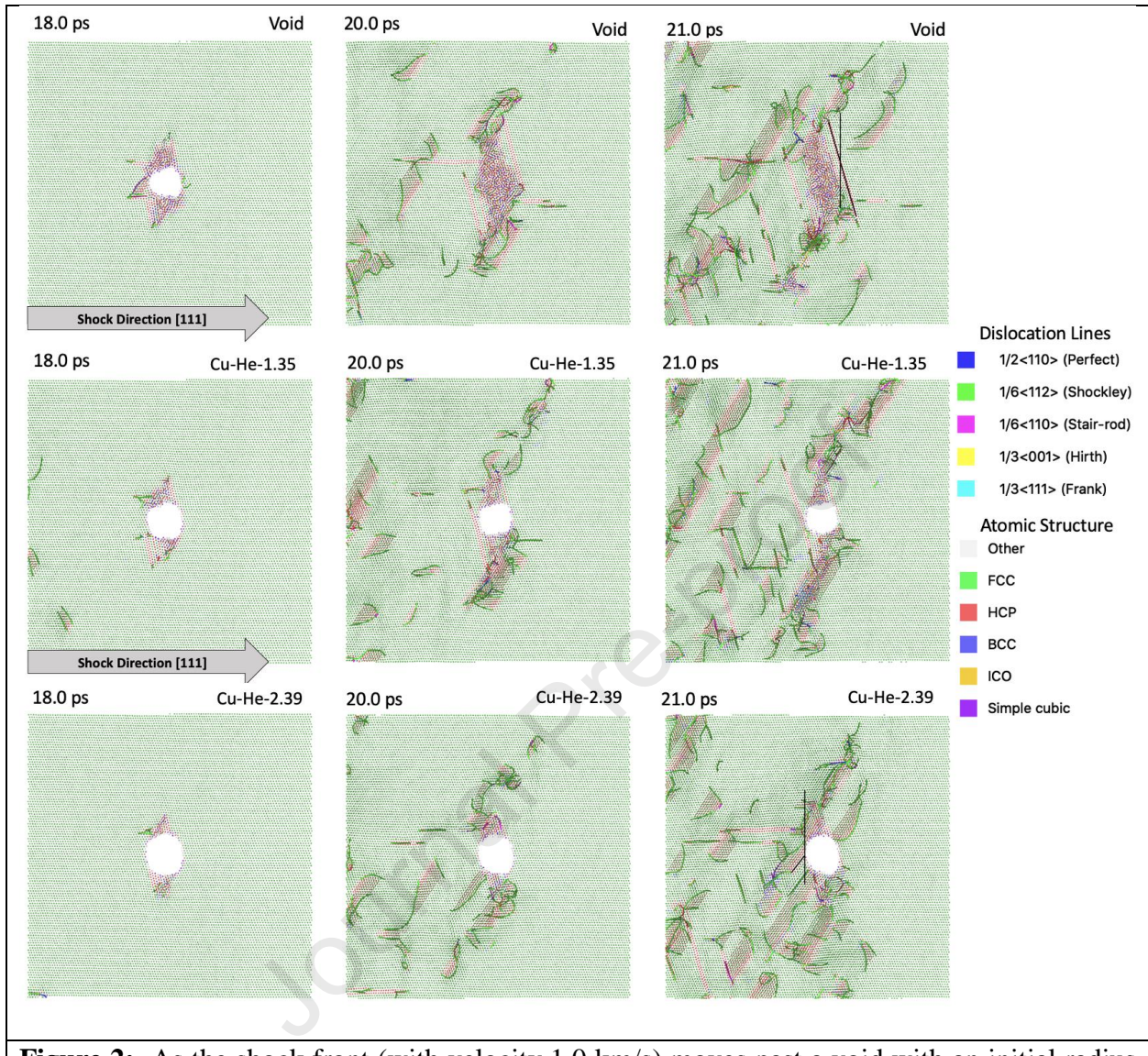


Figure 2: As the shock front (with velocity 1.0 km/s) moves past a void with an initial radius of 2 nm, dislocations are emitted from the void. Figures a-c show the full collapse of the empty void under shock loading, where a significant number of Shockley partial dislocations are emitted. Figures d-f show the helium bubble in Cu-He-1.35 does not collapse under shock loading, emitting less dislocations. This effect is more pronounced in figures g-i, depicting Cu-He-2.39.

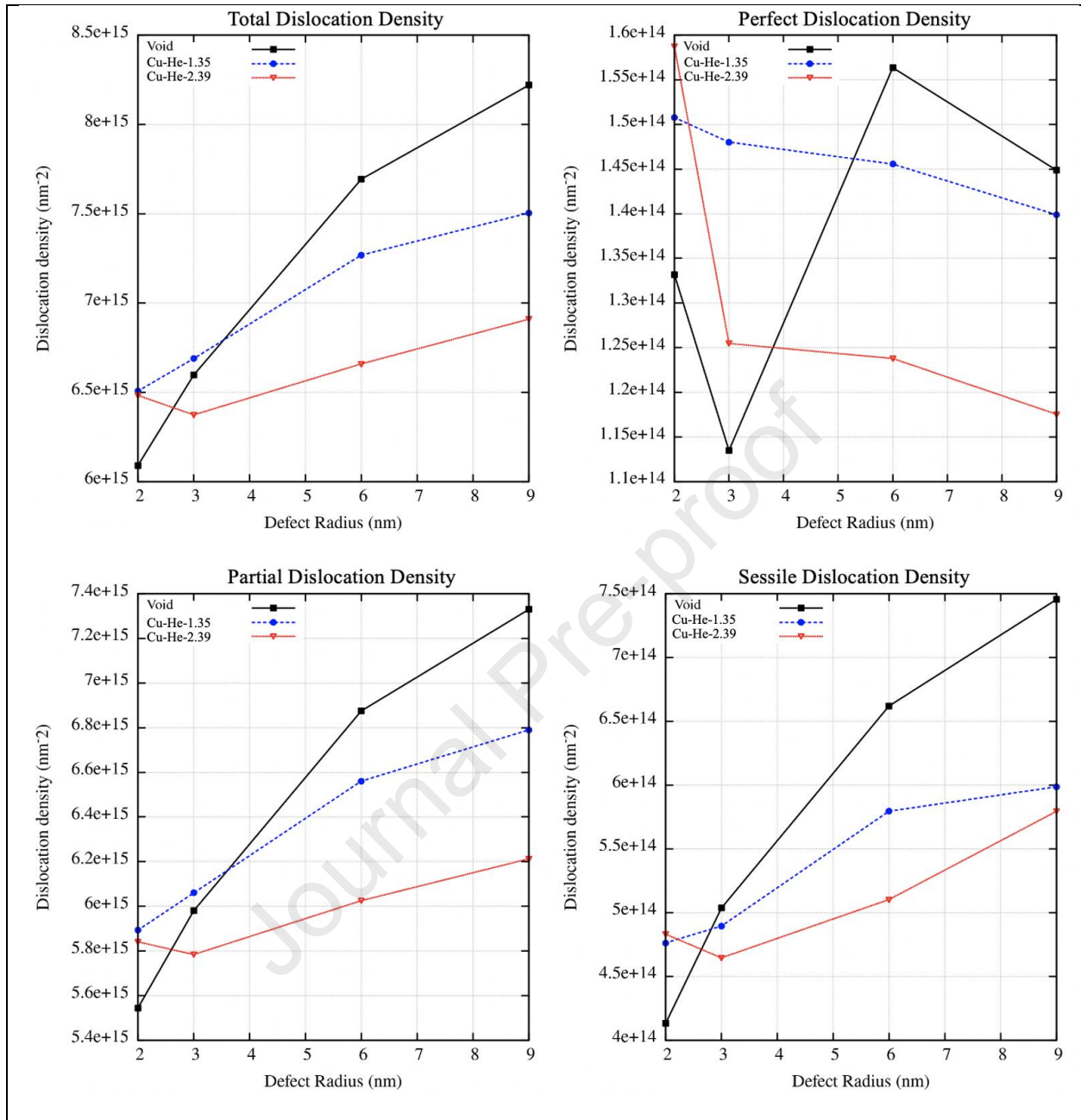


Figure 3: The dislocation density around void as a function of void size for voids subjected to a peak pressure of 48 GPa. Figure a shows the total dislocation density. Figure b illustrates the dislocation density for perfect dislocations. Figure c shows the dislocation density for Shockley partials while figure d shows the dislocation density of sessile dislocations, including stair-rod, Hirth, and Frank dislocations. For small voids, He-filled defects tend to produce more

dislocations than the empty void, but as the void size increases, the empty void produces remarkably more dislocations, likely due to its full collapse.

Journal Pre-proof

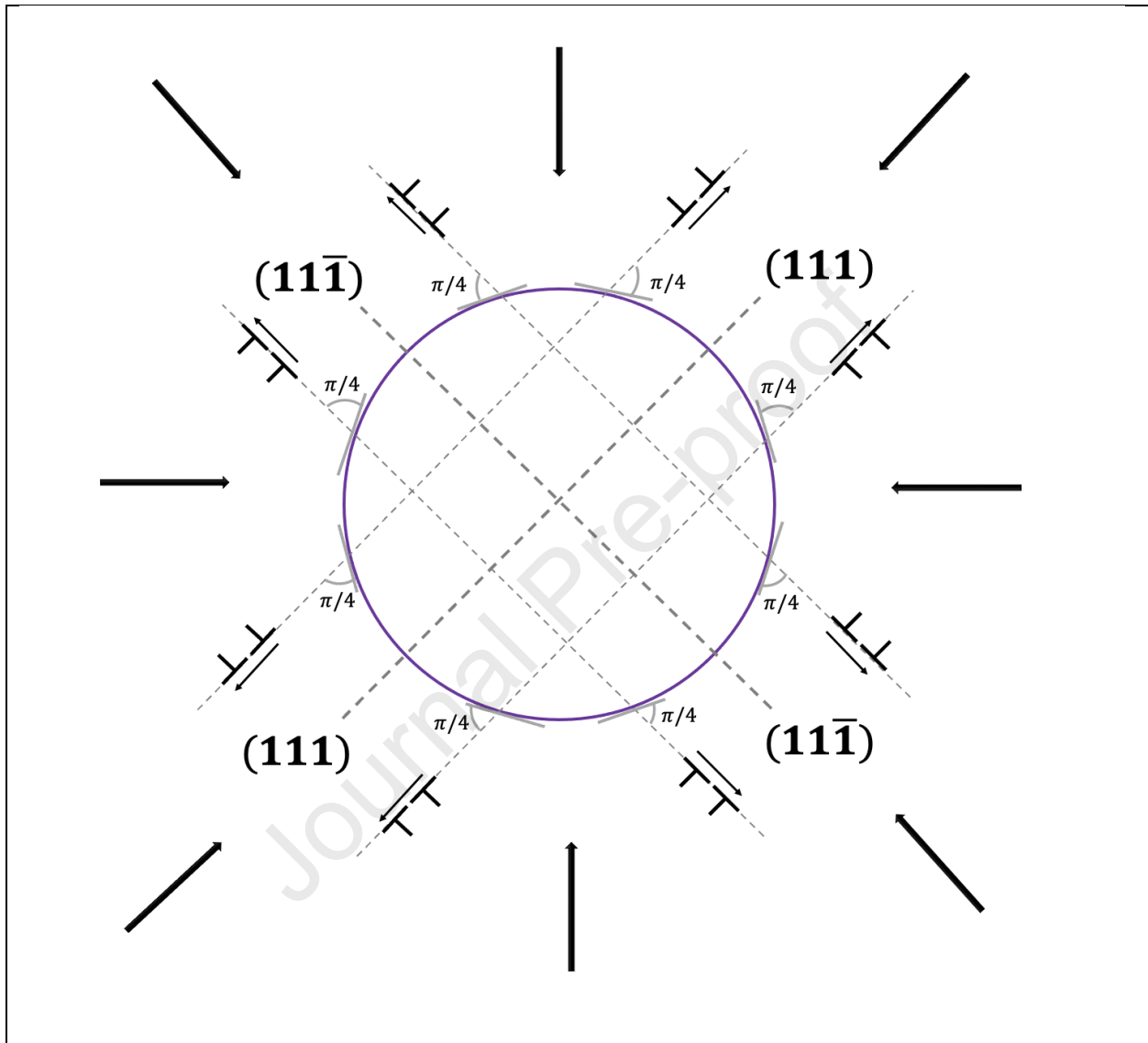
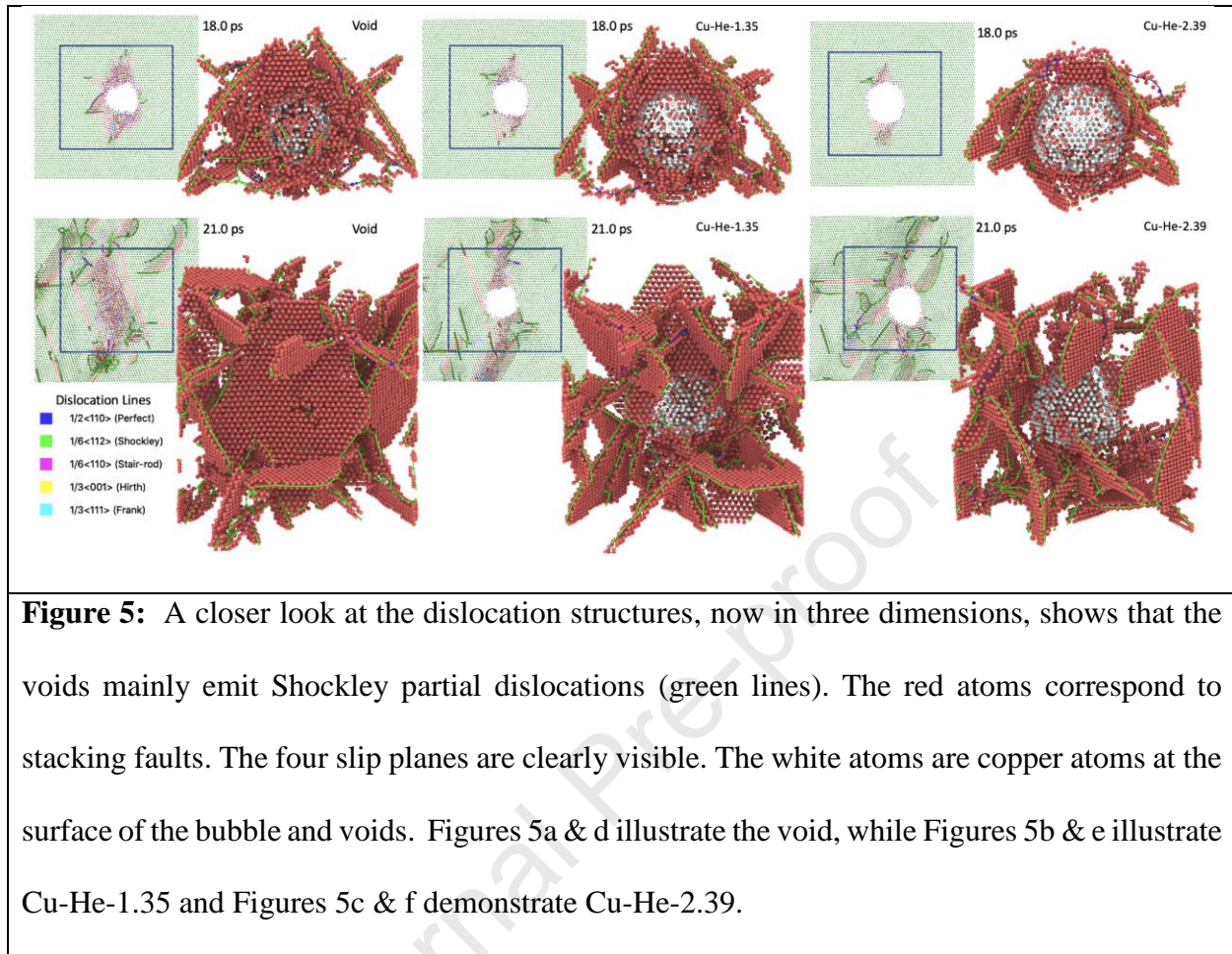


Figure 4: Positions of maximum shear stress on the surface of a void in biaxial compression with two slip planes ((111) and $(\bar{1}\bar{1}\bar{1})$). Emission of dislocations at these points, leading to a decrease of void volume.



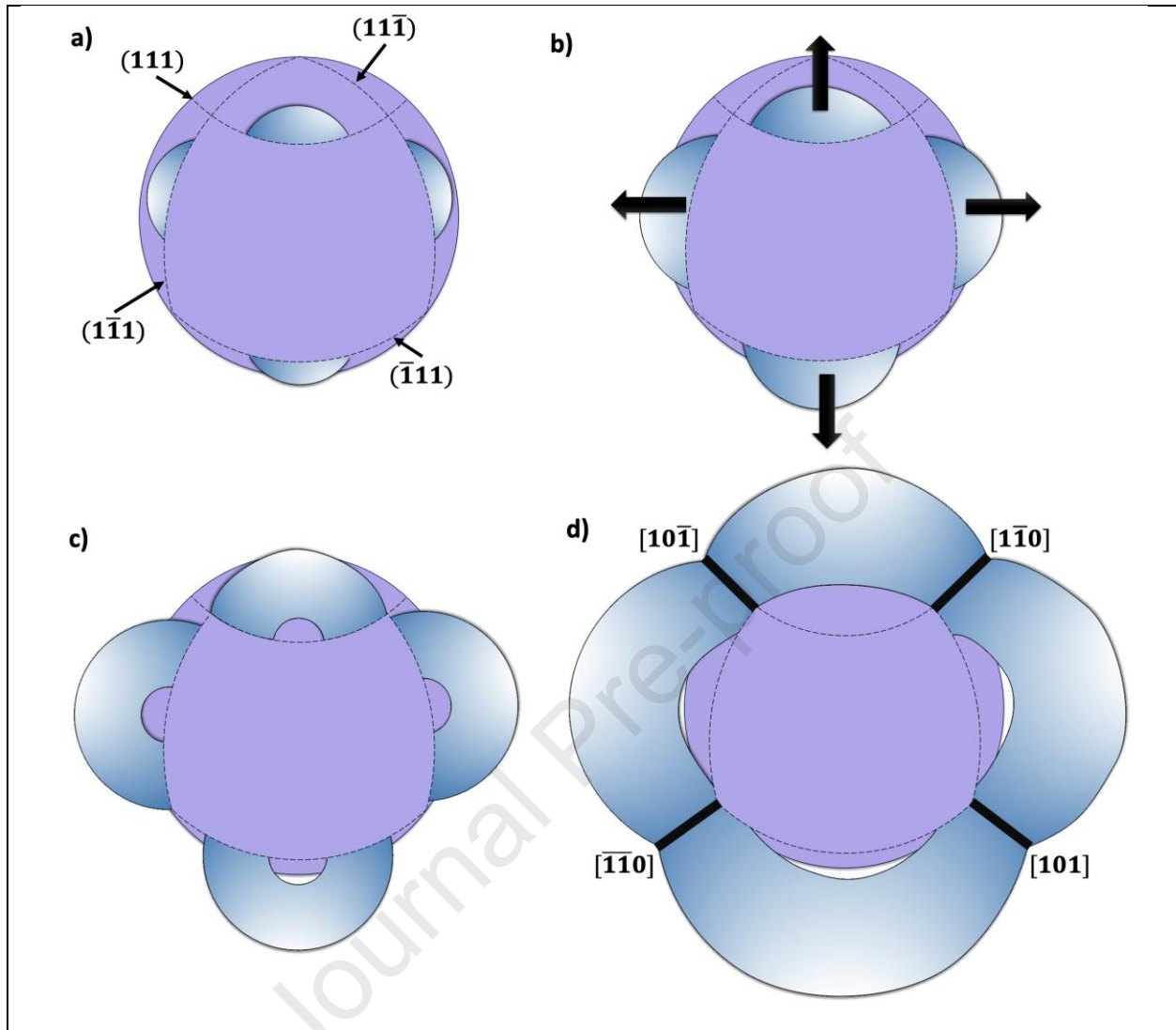
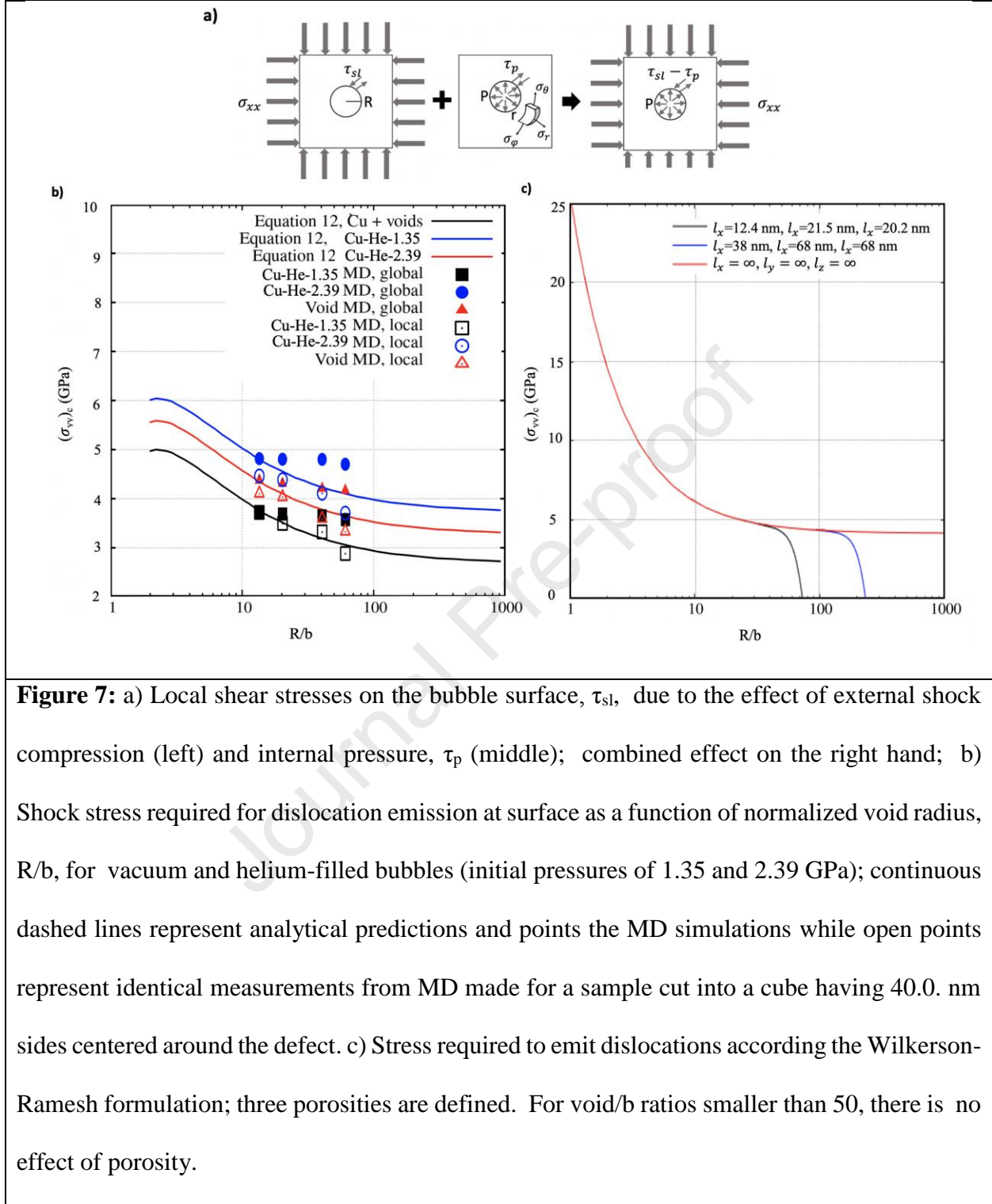


Figure 6: Schematic representation of emission of shear dislocation loops in blue during collapse of a void whose surface is colored purple; four non-perpendicular slip planes $((111), (\bar{1}\bar{1}1), (11\bar{1}), \text{and } (1\bar{1}1))$ are shown; (a) planes of maximum shear shown with the initiation of partial edge dislocation emission; (b) continued evolution of leading partials on four planes; (c) trailing partial emitted; (d) intersection of leading partials along directions $[110]$ (for (111) and $(11\bar{1})$), $[10\bar{1}]$ (for (111) and $(1\bar{1}1)$), $[101]$ (for $(11\bar{1})$ and $(\bar{1}\bar{1}1)$); $[\bar{1}10]$ for $(1\bar{1}1)$ and (-111) . $(111), (11\bar{1}), (\bar{1}\bar{1}1)$ and $(1\bar{1}1)$



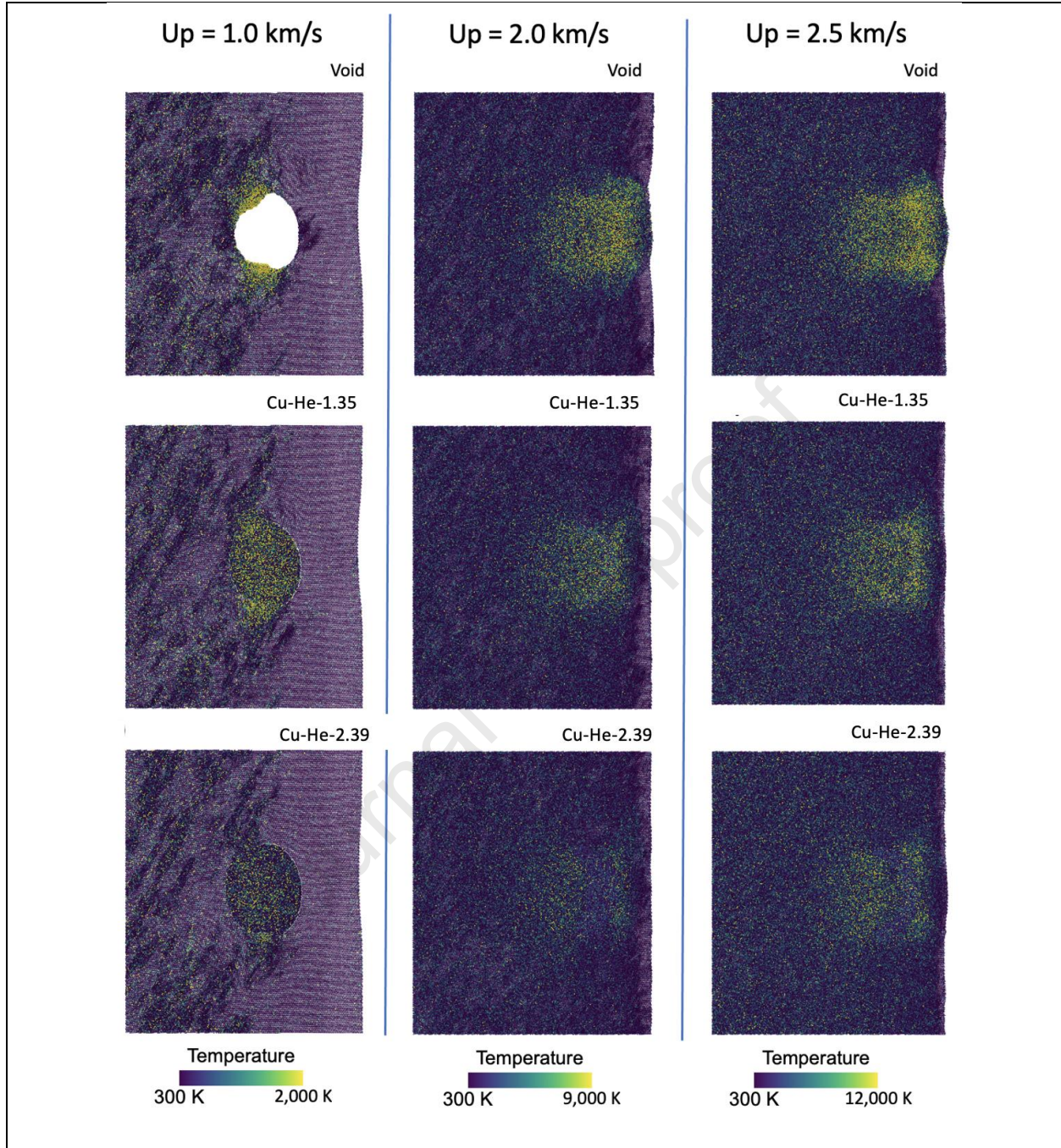


Figure 8: Localized temperature of void having a radius of 9.0 nm under shock compression at the time that the shock front has reached the rear surface. While hot spots clearly form in the case of empty voids, the distribution of the kinetic energy is more localized within the helium-filled voids.

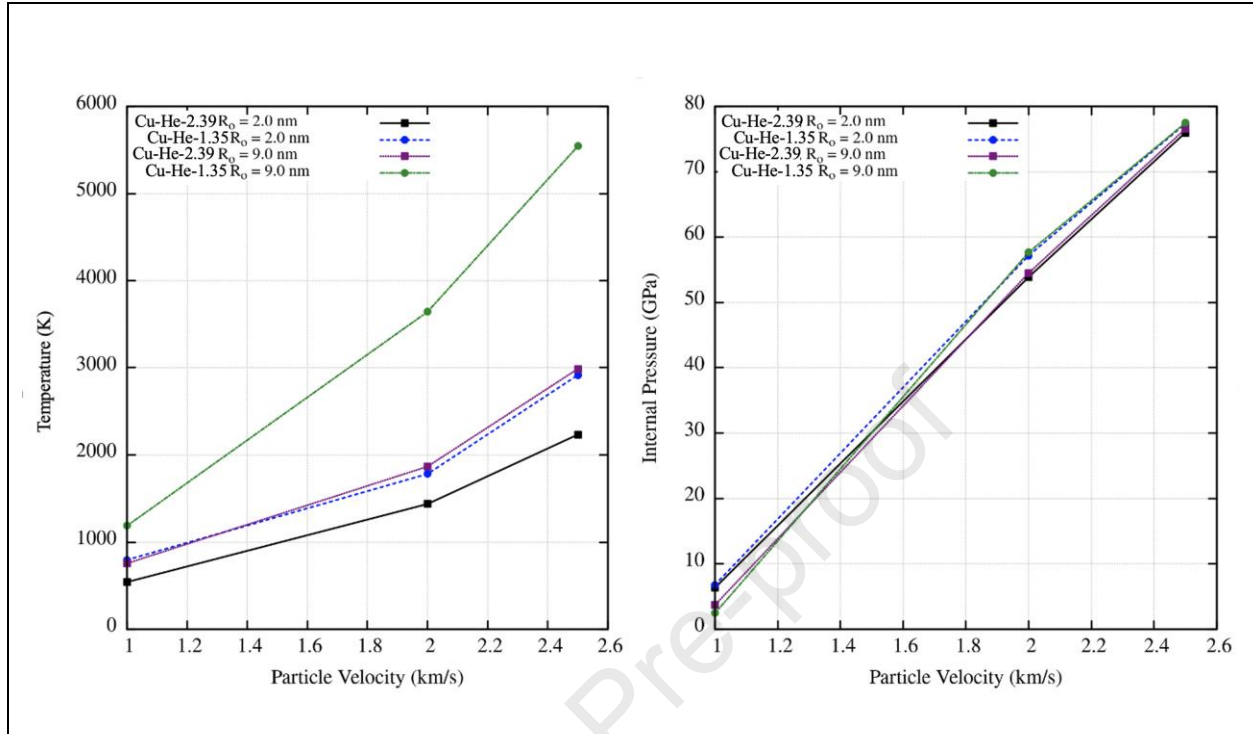


Figure 9: a) The temperature of each helium bubble, all of which remain intact during shock compression as function of particle velocity. b) The internal pressure of each helium bubble as a function of particle velocity. Note that empty voids collapse fully during shock compression so their temperature and pressure is indeterminate from the bulk copper.

Collapse of Helium-filled Voids in Extreme Deformation: Dislocation Mechanisms

R.M. Flanagan¹, M.A. Meyers¹, S.M. Valone², and S.J. Fensin^{2, *}

1. University of California, San Diego, CA

2. Los Alamos National Laboratory, Los Alamos, NM

* Corresponding Author

- Shock compression studies on single crystal Cu with pre-existing voids and helium bubbles generate localized, increased shear dislocation loops
- Varying size and internal pressure alters dislocation loop generation; as loops grow and interact, complex networks of sessile dislocations are formed
- The threshold shock stress is calculated via both analytical and computational means and reflects a clear trend of decreasing stress with increasing radius is observed; additionally, the critical shock stress for emission of dislocations around helium filled bubbles is higher than that of empty voids.

Declaration of interests

The authors declare that they have no known competing financial interests or personal relationships that could have appeared to influence the work reported in this paper.

The authors declare the following financial interests/personal relationships which may be considered as potential competing interests:

Journal Pre-proof